Research in Astronomy and Astrophysics, 24:065001 (8pp), 2024 June https://doi.org/10.1088/1674-4527/ad3f57

Dynamical Dark Energy in Light of Cosmic Distance Measurements. I. A Demonstration Using Simulated Datasets

Gan Gu[1,2], Xiaoma Wang[1,2], Xiaoyong Mu[1,2], Shuo Yuan[1], and Gong-Bo Zhao[1,2,3]
[1] National Astronomical Observatories, Chinese Academy of Sciences, Beijing 100101, China; gbzhao@nao.cas.cn
[2] University of Chinese Academy of Sciences, Beijing 100049, China
[3] Institute for Frontiers in Astronomy and Astrophysics, Beijing Normal University, Beijing 102206, China
Received 2024 April 7; accepted 2024 April 15; published 2024 May 24

Abstract

We develop methods to extract key dark energy information from cosmic distance measurements including the BAO scales and supernova (SN) luminosity distances. Demonstrated using simulated data sets of the complete DESI, LSST and Roman surveys designed for BAO and SN distance measurements, we show that using our method, the dynamical behavior of the energy, pressure, equation of state (with its time derivative) of dark energy and the cosmic deceleration function can all be accurately recovered from high-quality data, which allows for robust diagnostic tests for dark energy models.

Key words: (cosmology:) dark energy – (cosmology:) large-scale structure of universe – (cosmology:) cosmic background radiation – (cosmology:) cosmological parameters

1. Introduction

The physical origin of the accelerating expansion of the Universe, which was discovered using observations of type Ia supernovae (SNe Ia) in 1998 (Riess et al. 1998; Perlmutter et al. 1999), remains unknown. Possible mechanisms for the cosmic acceleration include dark energy (Copeland et al. 2006), which is a dominating component of the cosmic energy budget today with a negative pressure, and modified gravity (Clifton et al. 2012), a framework in which Einstein's general relativity (GR) gets modified. In both scenarios, an effective equation of state of dark energy, w, defined as a ratio of the pressure P over energy density ρ of the effective dark fluid, is a critical quantity for investigating models that can explain the cosmic acceleration. For example, $w=-1$ may mean that dark energy is essentially the vacuum energy, while an evolving w with cosmic time may suggest the dynamical nature of dark energy, or a breakdown of GR on cosmic scales. Therefore a direct reconstruction of w as a function of the scale factor a (or redshift z) from observations is of general interest (Sahni & Starobinsky 2006; Clarkson & Zunckel 2010; Holsclaw et al. 2010; Crittenden et al. 2012; Seikel et al. 2012; Zhao et al. 2012, 2017).

However, a reconstruction of $w(a)$ is not straightforward. Parametric reconstructions are easier to perform given the small number of free parameters to be determined, but the resultant reconstruction may be biased as it can only take the functional form assumed in the first place, which may not be appropriate. Non-parametric reconstructions are more general, but given the large number of degrees of freedom in the process, various kinds of data sets, such as the cosmic microwave background (CMB) (Spergel et al. 2003; Aghanim et al. 2020), SNe Ia (Riess et al. 1998; Perlmutter et al. 1999), baryonic acoustic oscillations (BAO) (Eisenstein & Hu 1998; Cole et al. 2005; Eisenstein et al. 2005; Alam et al. 2021) and redshift space distortions (RSD) (Kaiser 1987; Peacock et al. 2001; Alam et al. 2021), are combined for the purpose of degeneracy breaking. If one or more kinds of data sets are contaminated by unknown systematics, which is not impossible, the final reconstructed $w(a)$ inherits the systematics. In this sense, it is better to learn $w(a)$ from each individual type of data set, and cross check the consistency, especially when data sets are in tension. But unfortunately, this is difficult for non-parametric reconstruction methods.

Actually, one can learn important features of $w(a)$ without a direct reconstruction. In this work, we derive useful diagnostic quantities for $w(a)$ from cosmic distance measurements including the BAO scales and SN Ia luminosity distances, and validate our tests using simulated data sets including the galaxy survey of Dark Energy Spectroscopic Instrument (DESI) (Aghamousa et al. 2016) and SN Ia surveys of Rubin Observatory's Legacy Survey of Space and Time (LSST) (LSST Science Collaboration et al. 2009) and the Roman Space Telescope (Spergel et al. 2015).

This paper is structured as follows. We develop the methodology in Section 2, describe the simulated data sets in Section 3, and present the main result in Section 4, before concluding in Section 5. Some technical details are included in the Appendices.

2. Features of Dark Energy Hidden in Distance Measurements

In this section, we show the information content of cosmic distance measurements that is relevant for dark energy

studies, and propose methods to extract this piece of crucial information.

2.1. The Shape Function of Dark Energy

In a spatially flat Universe, the Hubble expansion rate $H(a)$ is related to the fractional dark energy density $X(a)$ through

$$f(a) \equiv AH^2a^3 = B[X(a)a^3] + C, \tag{1}$$

where A, B and C are constants. For example, for BAO observables, $A = r_d^2$, $B = r_d^2H_0^2(1 - \Omega_{\rm M})$, $C = r_d^2H_0^2\Omega_{\rm M}$ with H_0, r_d and $\Omega_{\rm M}$ being the Hubble constant, the sound horizon at decoupling, and the present-day fractional matter density, respectively. The quantity $X(a)$ is defined as,

$$X(a) \equiv \frac{\rho_{\rm DE}(a)}{\rho_{\rm DE}(a=1)} = \exp\left[-3\int_1^a \frac{1+w(y)}{y}dy\right], \tag{2}$$

where $\rho_{\rm DE}$ and w are the mean energy density and the equation of state of dark energy, respectively.

From Equation (1), it is clear that functions H^2a^3 and Xa^3 have the same shape, meaning that they are identical after a proper shift and normalization. For example,

$$S[AH^2a^3] = S[Xa^3];\ \ S[f(a)] \equiv \frac{f(a) - f(a_\star)}{f'(a_\star)}, \tag{3}$$

where $S[f(a)]$ defines a shape function of $f(a)$, and $a_\star$ is a reference scale factor. Throughout the paper, the superscript $'$ denotes a derivative with respect to the scale factor a. Although the choice of $a_\star$ is arbitrary, it makes sense to choose one so that $f'(a_\star)$ can be well measured, thus we can get a decent estimation for S and other quantities that depend on $f'(a_\star)$. For the simulated data sets used in this work, we find that $a_\star = 2/3$ is a reasonable choice to yield a tight constraint of $f'(a_\star)$ using either the BAO or SN data sets, so we set $a_\star = 2/3$ for all results in this paper. We can obtain the shape information of Xa^3 through $S[AH^2a^3]$, which is a direct observable, and can be used as a diagnostic for dark energy models. For example,

$$\Lambda{\rm CDM} \Longrightarrow S[AH^2a^3] = \frac{a^3 - a_\star^3}{3a_\star^2}. \tag{4}$$

2.2. The Pressure of Dark Energy

Since the pressure P of dark energy is proportional to wX, it follows that

$$R(a, a_\star) \equiv \frac{P(a)}{P(a_\star)} = \frac{w(a)X(a)}{w(a_\star)X(a_\star)} = \frac{a_\star^2}{a^2}\frac{f'(a)}{f'(a_\star)}, \tag{5}$$

where $a_\star$ denotes a reference point for a normalization. From the definition, it is clear that,

$$\begin{aligned} &w = -1 \Longrightarrow R = 1, \\ &w = \text{constant} \Longrightarrow R = \left(\frac{a}{a_\star}\right)^{-3(1+w)} \\ &\Longrightarrow \frac{\log R}{\log(a/a_\star)} = \text{constant}. \end{aligned} \tag{6}$$

2.3. The Characterization Function of Dark Energy

To obtain further information of $w(a)$, we take the second derivative of $f(a)$ with respect to a and compare it to $f'(a)$.[4] Specifically,

$$g(a) \equiv -\frac{1}{3}\left[a\frac{f''(a)}{f'(a)} + 1\right] = w - \frac{a}{3}\frac{w'}{w}. \tag{7}$$

This function is a direct observable from distance measurements (Alam et al. 2003; Sahni et al. 2003), and it contains only w and w'. This means that it is free from degeneracies with any other cosmological parameters such as $\Omega_{\rm M}$, H_0, etc. From the definition of $g(a)$, we see that,

$$\begin{aligned} &w = -1 \Longrightarrow g = -1, \\ &w = \text{constant} \Longrightarrow g = w = \text{constant}, \\ &\text{At high redshifts} \Longrightarrow g \simeq w, \\ &w \text{ slowly varies with time} \Longrightarrow g \simeq w, \\ &w = w_0 + w_a(1 - a) \Longrightarrow \\ &\ g \text{ is close to a linear function of } a. \end{aligned} \tag{8}$$

These features can be used as diagnostics for dark energy models. For example, $g \neq -1$ rules out the ΛCDM model, and a varying g with time rules out the wCDM model (the model in which w is a constant). Furthermore, given a measurement of $g(a)$, we can obtain a relation between w and w' at any redshift. This can in principle be used to differentiate dark energy models in the $w - w'$ phase-space (Caldwell & Linder 2005; Chiba 2009; Scherrer 2006), which is presented in a companion paper (Wang et al. 2024).

2.4. The Deceleration Function

The deceleration function $q(a)$ is another useful quantity that can be derived from $f(a)$, although it is not solely dependent on dark energy parameters. Specifically,

$$q(a) \equiv -a\frac{H'}{H} - 1 = \frac{1}{2}\left[1 - \frac{af'(a)}{f(a)}\right]. \tag{9}$$

[4] An explicit derivation is included in Appendix A.

Table 1
Dark Energy Models Used for Producing the Mock Datasets

Dark Energy Models	$w(a)$
ΛCDM	$w=-1$
wCDM	$w=-0.82$
CPL	$w=-0.9-0.8(1-a)$
POLY	$w=-1.1-1.3(1-a)+11.2(1-a)^2-15.7(1-a)^3$

2.5. The Parameterization of the Cosmic Distances

All the above-mentioned useful functions can be derived from $f(a)$, thus it is important to derive $f(a)$ from distance measurements in an efficient and accurate way. Following Zhu et al. (2015), we parameterize the cosmological distances in the form of,

$$\frac{D_{\rm A}(a)}{D_{\rm A,\,fid}(a)}=\alpha_0\Bigg(1+\alpha_1 x+\frac{1}{2}\alpha_2 x^2+\frac{1}{6}\alpha_3 x^3+\frac{1}{24}\alpha_4 x^4+\frac{1}{120}\alpha_5 x^5+\frac{1}{720}\alpha_6 x^6\Bigg),$$
$$x\equiv\frac{\chi_{\rm fid}(a)}{\chi_{\rm fid}(a_{\rm p})}-1, \quad (10)$$

where $a_{\rm p}$ is the pivot point for the expansion, and we choose to set $a_{\rm p}=2/3$ in this work. As demonstrated in Appendix B.1, the choice of $a_{\rm p}$ has almost no impact on the final reconstruction result. Since Equation (10) is essentially a Taylor expansion, we need a criterion to determine the maximal order of expansion to be included in the series. Keeping more terms in the expansion makes this parametric reconstruction more accurate, but this also inflates the uncertainties due to the degeneracies among parameters. Therefore a balance between the reconstruction bias and the statistical uncertainties is required when determining the highest order of the expansion. Note that this depends on the data set being used—better measured data can help to constrain more parameters. Given the sensitivity of DESI, LSST and Roman, we find that keeping terms α_0 to α_6 in the expansion is a sensible choice when all data sets are combined[5] for the four fiducial dark energy models considered in this work (see a demonstration in Appendix B.2), which cover a wide range of phenomenological dark energy models.

The subscript "fid" stands for the fiducial cosmology, which is chosen to be a ΛCDM model favored by the latest Planck observations (Planck Collaboration et al. 2020). Using the relation between H and $D_{\rm A}$ in a flat Universe, we find that,

$$\frac{H_{\rm fid}(a)}{H(a)}=\beta_0(1+\beta_1 x+\beta_2 x^2+\beta_3 x^3+\beta_4 x^4+\beta_5 x^5+\beta_6 x^6), \quad (11)$$

[5] For the case of BAO alone, we keep terms α_0 to α_4 to avoid overfitting.

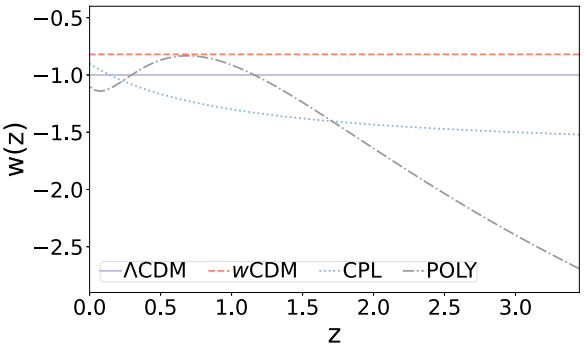

Figure 1. The $w(z)$ models used as fiducial models in this work.

where parameters β_i can be derived from α_i, and an explicit derivation is included in Appendix C. Equations (10) and (11) allow for a parametric reconstruction of $f(a)$ from distance measurements[6], including the BAO distance measurements,[7] the luminosity distance measurements from SN Ia observations, and $H(z)$ measurements from the cosmic chronometers (Stern et al. 2010).

3. Simulated Datasets and Parameter Estimation

In this section, we present the simulated data sets used for this work, including the mock BAO data sets for the complete DESI survey, and the mock SN Ia data sets assuming a sensitivity of the LSST and Roman surveys.

To start with, we choose four phenomenological dark energy models as fiducial models shown in Table 1 and Figure 1. These include the ΛCDM model ($w=-1$), a wCDM model with $w=-0.82$, a Chevallier–Polarski–Linder (CPL) model (Chevallier & Polarski 2001; Linder 2003) with $w_0=-0.9$ and $w_a=-0.8$, and a more complicated model of $w(a)$, which is a polynomial of $(1-a)$ (POLY). To be generic, the parameters for the CPL and POLY models are chosen so that $w(a)$ is allowed to cross the $w=-1$ boundary, as motivated by observations (Feng et al. 2005; Zhao et al. 2012, 2017; Wang et al. 2018; Adame et al. 2024). Throughout the paper we assume fiducial values of $\Omega_{\rm M}=0.315$ and $H_0=67.4\,{\rm km\,s^{-1}\,Mpc^{-1}}$, which are consistent with values in a ΛCDM model favored by Planck observations (Aghanim et al. 2020). Given the input dark energy models and fiducial values of $\Omega_{\rm M}$ and H_0, the simulated BAO and SN Ia observables, including the mean values and data covariance matrix, can be created, if the sensitivity of the relevant surveys is assumed.

[6] Note that when fitting α's in Equations (10) and (11) to distance measurements, the derived X may not be positive-definite. Therefore when deriving quantities related to f' including the pressure function and the g function, we apply a prior of $X>0$. We check the posteriors and find that this has a marginal effect on the final result.

[7] Note that galaxy surveys provide BAO distance measurements of $D_{\rm A}/r_d$, Hr_d or $D_{\rm V}/r_d$, instead of $D_{\rm A}$, H or $D_{\rm V}$, but this does not matter since the unknown amplitude r_d can be absorbed into α_0 or β_0. As we only use the shape information of $f(a)$ for dark energy studies, the values of α_0 or β_0 are actually irrelevant.

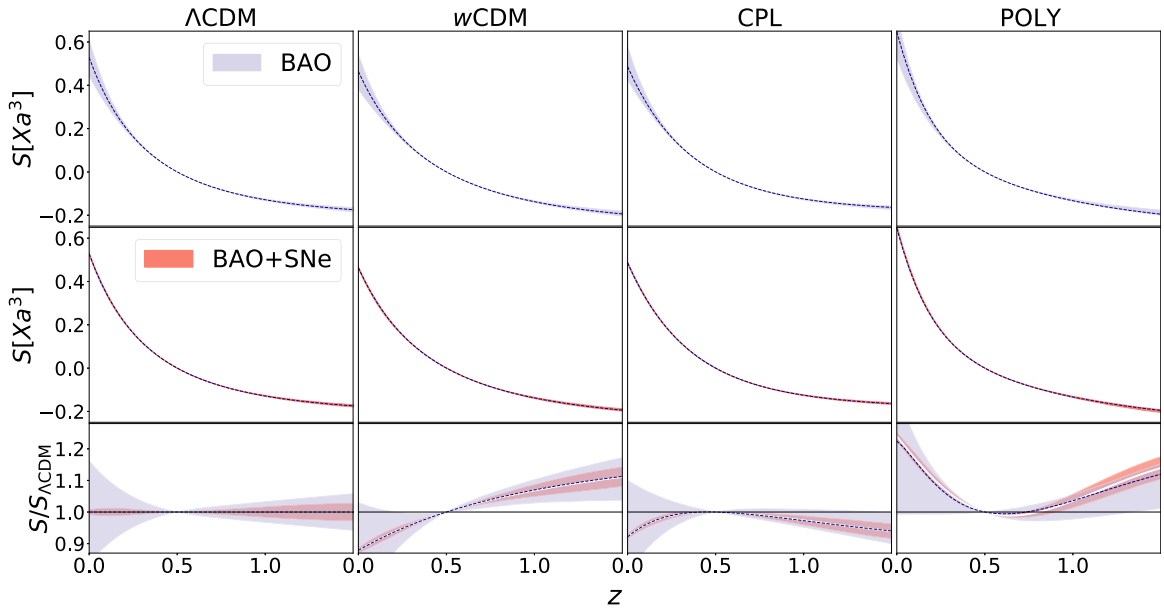

Figure 2. The reconstructed shape function of dark energy, $S[Xa^3]$, as a function of redshift z for four input $w(z)$ models as illustrated in the legend. In all panels, the blue dashed lines represent the input model, and the shaded bands show the 68% confidence level (CL) reconstruction. The top and middle panels present results derived from the simulated BAO assuming a complete DESI survey (blue bands) and BAO combined with SN data sets assuming complete LSST and Roman surveys (red bands), respectively. The bottom panel shows the result normalized by the ΛCDM model $S_{\Lambda\mathrm{CDM}}$. The white curves in the middle correspond to the mean of the reconstructed S function.

3.1. Simulated BAO Observables

For the BAO observables, we assume a sensitivity of the complete DESI survey. DESI is a Stage IV ground-based galaxy spectroscopic survey, measuring the expansion rate and the growth rate of cosmic structures at (sub)percent level across a wide range of redshifts. We follow the official DESI specifications (DESI Collaboration et al. 2023), and use the forecast sensitivity of D_{A}/r_d and Hr_d derived from tracers including the Bright Galaxy Samples (BGS), Luminous Red Galaxies (LRGs), Emission Line Galaxies (ELGs), Quasars (QSOs) and the Lyα forest (Lyα) at $0 < z < 3.5$.

3.2. Simulated SN Ia Observables

SNe Ia, as cosmic standard candles, offer measurements of luminosity distances at multiple redshifts. LSST (LSST Science Collaboration et al. 2009) and Roman (Spergel et al. 2015) are two main forthcoming SN Ia surveys with complementary redshift coverage, namely, LSST aims to observe hundreds of thousands of SNe at low and intermediate redshifts, while Roman is expected to detect SNe up to $z = 3$. We assume that the uncertainties of the SN distance modulus are quadratic sums of the intrinsic scatter of $\sigma_{\mathrm{int}} = 0.13$ mag and both the lensing-induced scatter and the peculiar velocity scatter.[8] For the expected number of SNe to be detected by LSST, we follow Matos et al. (2023) to assume a 10 yr survey over 18,000 deg^2 with a 15% completeness at $z < 0.7$, and for Roman, we assume a WIDE survey mode (Rose et al. 2021).

[8] We assume ideal cases with no systematics in this simulation.

3.3. Parameter Estimation

Given the simulated data sets, which include a data vector storing the mean value of the observables, and a data covariance matrix, we perform a Markov Chain Monte Carlo (MCMC) analysis to constrain the α parameters defined in Equation (10) using the `Cobaya` software (Torrado & Lewis 2021).

4. Results

In this section, we present the main result of this work, as summarized in Figures 2–5.

Figure 2 shows the reconstructed shape function of Xa^3, derived from the simulated DESI BAO data alone (top panels) and from the simulated DESI BAO + LSST (SNe) + Roman (SNe) (middle panels). For a better visualization, we show the result normalized by S predicted by the ΛCDM model in the bottom panel. As demonstrated, the input models (drawn in dashed blue curves) are well recovered in all cases, validating our pipeline for reconstructing $S[Xa^3]$ from data. We find that forthcoming BAO combined with SN observations can well constrain the shape function of dark energy, making it possible to use this function to test the ΛCDM model to a high precision.

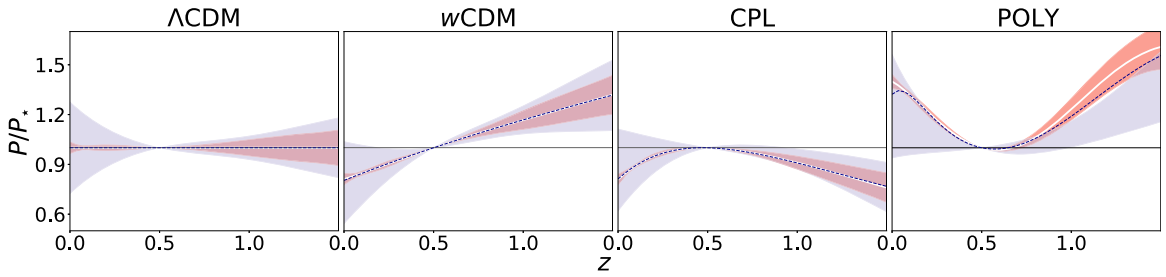

Figure 3. The reconstructed pressure function of dark energy, normalized at $a = a_\star$, as a function of redshift z for four input $w(z)$ models as illustrated in the legend. In all panels, the blue dashed lines represent the input model, and the shaded bands show the 68% confidence level (CL) reconstruction derived from the simulated BAO (blue bands) and BAO combined with SN data sets (red bands), respectively. The horizontal black lines show the ΛCDM prediction of $P/P_\star = 1$ for a reference.

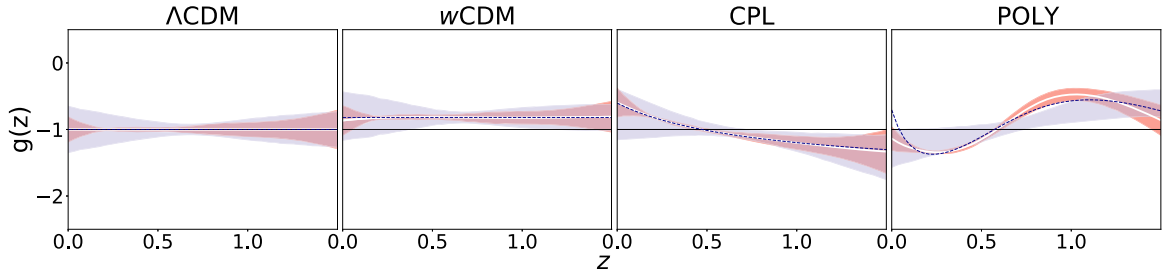

Figure 4. Same as Figure 3, but for $g(z)$. The horizontal black lines show the ΛCDM prediction of $g = -1$ for a reference.

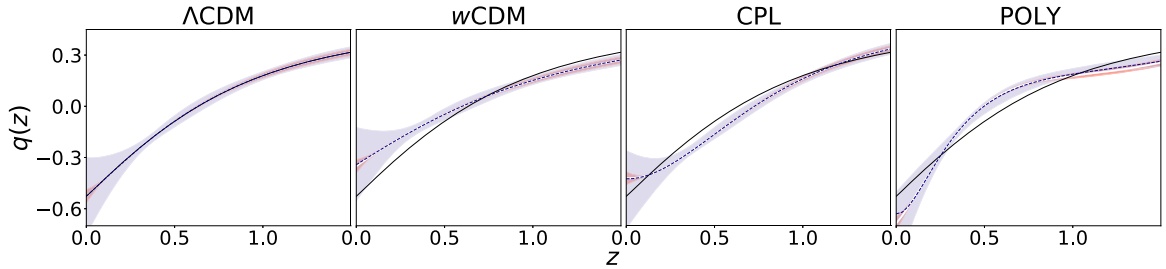

Figure 5. Same as Figure 4, but for the deceleration function $q(z)$. The black lines show the ΛCDM prediction for a reference.

Figures 3–5 depict the reconstructed pressure function $P(z)$ of dark energy (normalized by the value of P at $a_\star$), the characterization function $g(z)$, and the deceleration function $q(z)$, respectively. As shown, all input models can be recovered at $z \gtrsim 0.1$ within the small uncertainties derived from the simulated data sets of BAO (DESI) + SNe (LSST+Roman). The POLY model is less well reproduced at $z \lesssim 0.1$ due to its wiggly feature at such low redshifts, which requires higher-order terms in the expansion in Equation (10). We have tried an expansion of Equation (10) with the α_7 term (see Appendix B.2), which indeed improves the accuracy of the reconstruction, but with much larger uncertainties. Therefore, our default choice (keeping up to the α_6 term) is a reasonable compromise.

5. Conclusion and Discussions

In this era of precision cosmology, we have been gaining access to high quality observational data probing the Universe from various angles, which is deepening our understanding of the cosmos. Revealing the nature of dark energy is one of the most challenging problems to tackle in modern cosmology. As dark energy is the driving force of the current acceleration of the spacetime expansion, it is crucial to develop methods and tools to capture critical features of dark energy from measurements of the cosmic expansion.

In this work, we develop methods to extract important features of dark energy, including the shape function of dark energy $S[Xa^3]$, the evolution history of the pressure $P(a)/P(a_\star)$,

the characterization function $g(a)$, and the deceleration function $q(a)$, from cosmic distance measurements, primarily including BAO and SN measurements. We apply our pipeline to simulated DESI, LSST and Roman data sets created for a range of phenomenological dark energy models, and find that our method can well capture the dynamical features of dark energy hidden in the simulated data sets. As our method only extracts information of dark energy from distance measurements, it is by design free from degeneracies among other cosmological parameters. This allows for diagnostic dark energy tests using individual type of observational data, which is important for dark energy studies.

Our method is directly applicable to existing cosmic distance measurements for dark energy tests, which is released in a companion paper (Wang et al. 2024).

Acknowledgments

We thank Ruiyang Zhao for helpful discussions. All authors are supported by the National Key R & D Program of China (2023YFA1607800, 2023YFA1607803), the National Natural Science Foundation of China (NSFC, Grant Nos. 11925303 and 11890691), and by a CAS Project for Young Scientists in Basic Research (No. YSBR-092). S.Y. is also supported by the National Natural Science Foundation of China (NSFC, Grant No. 12203062). S.Y. and G.B.Z. are also supported by science research grants from the China Manned Space Project with No. CMS-CSST-2021-B01. G.B.Z. is also supported by the New Cornerstone Science Foundation through the XPLORER prize.

Appendix A
Derivation of the Characterization Function

By definition,

$$f(a) \equiv H^2 a^3 = H_0^2[\Omega_{\rm M} + (1 - \Omega_{\rm M})X(a)a^3]. \quad \text{(A1)}$$

Then

$$\begin{aligned} f'(a) &= \frac{d}{da}H_0^2[\Omega_{\rm M} + (1 - \Omega_{\rm M})X(a)a^3] \\ &= -3H_0^2(1 - \Omega_{\rm M})w(a)X(a)a^2, \end{aligned} \quad \text{(A2)}$$

Thus

$$\frac{f''(a)}{f'(a)} = \frac{1}{a}\left[a\frac{w'(a)}{w(a)} - 3w(a) - 1\right]. \quad \text{(A4)}$$

Hence,

$$g(a) \equiv w - \frac{a}{3}\frac{w'}{w} = -\frac{1}{3}\left[a\frac{f''(a)}{f'(a)} + 1\right]. \quad \text{(A5)}$$

Appendix B
Choice of the Pivot Point and Order of the Expansion

B.1. Impact of the Choice of z_p *on the Reconstructed* f

We test how the choice of $z_{\rm p}$ affects the reconstructed dark energy shape function f, as defined in Equation (3). For this test, we reconstruct f from the simulated DESI data created with various dark energy models with four choices of $z_{\rm p}$ of 0.2, 0.4, 0.6 and 0.8, and show the result in Figure B1. As expected, the choice of $z_{\rm p}$ has negligible effect on the final reconstructed f, which demonstrates the robustness of our reconstruction result.

B.2. Impact of the Expansion Order

The maximum order of the expansion in Equation (10) does affect the final reconstruction of the functions that are closely related to dark energy. As a demonstration, in Figure B2 we show the reconstructed $g(a)$ from the simulated DESI+LSST +Roman data sets for the POLY model with different maximum orders of expansion, namely, we use expansions up to the x^5 ($O5$), x^6 ($O6$) and x^7 ($O7$) terms in Equation (C1), respectively. As shown, the reconstruction bias is significant in the $O5$ case, while the uncertainties are large in the $O7$ case, making the $O6$ case a reasonable compromise, which is used for producing the main results of this work.

$$\begin{aligned} f''(a) &= -3H_0^2(1 - \Omega_{\rm M})\frac{d}{da}[w(a)X(a)a^2] \\ &= -3H_0^2(1 - \Omega_{\rm M})\left[w'(a)X(a)a^2 + w(a)X(a)(-3)\frac{1 + w(a)}{a}a^2 + w(a)X(a)2a\right] \\ &= -3H_0^2(1 - \Omega_{\rm M})[a^2 w'(a)X(a) - aw(a)X(a) - 3aw^2(a)X(a)]. \end{aligned} \quad \text{(A3)}$$

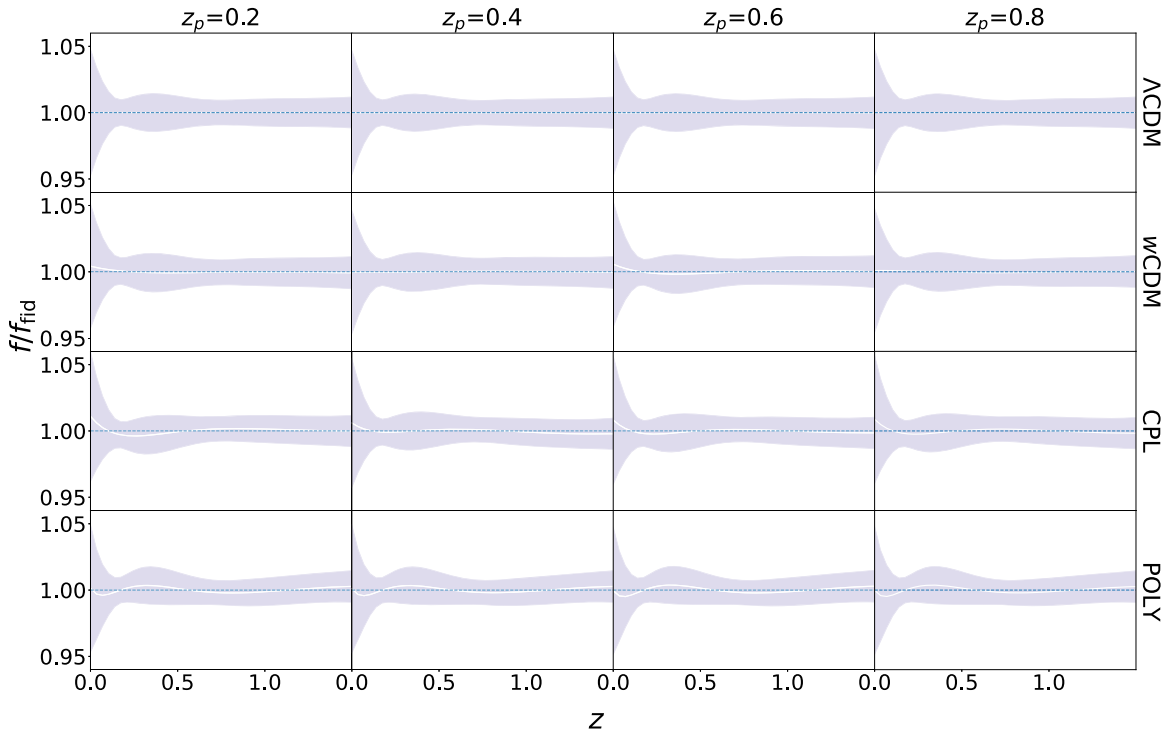

Figure B1. The reconstructed dark energy shape function f normalized by the input fiducial function for four different choices of $z_{\rm p}$. The mean (white lines) and 68% CL uncertainties (shaded regions) derived from the simulated DESI data are shown for four phenomenological dark energy models illustrated in the legend. The horizontal blue dashed lines show $f/f_{\rm fid} = 1$ for a reference.

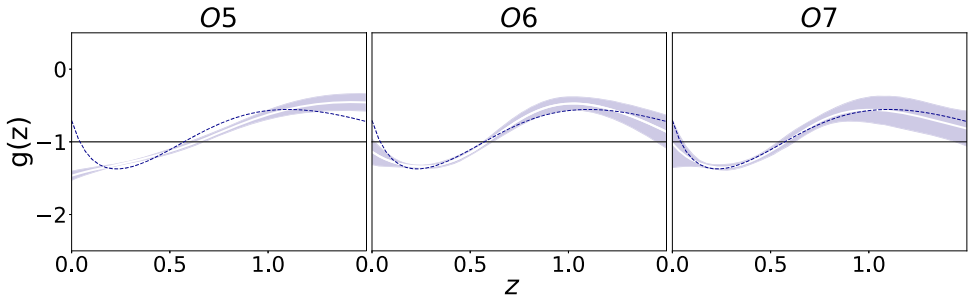

Figure B2. The mean (white lines) and 68% CL uncertainties (shaded regions) of the reconstructed g function of the POLY fiducial model using expansions up to the x^5 ($O5$), x^6 ($O6$) and x^7 ($O7$) terms in Equation (C1). The blue dashed lines represent the input fiducial model, and the black horizontal lines show the ΛCDM prediction for a reference.

Appendix C
Derivation of the Distance-redshift Parameters

To be general, we expand $\chi/\chi_{\rm fid}$ up to order N, namely,

$$\chi(z) = \alpha_0\left(1 + \sum_{i=1}^{N}\frac{1}{i!}\alpha_i x^i\right)\chi_{\rm fid}(z), \tag{C1}$$

where

$$x \equiv \chi_{\rm fid}(z)/\chi_{\rm fid}(z_{\rm p}) - 1. \tag{C2}$$

Taking the derivative of Equation (C1) with respect to z, we have

$$\begin{aligned}\frac{1}{H(z)} &= \frac{d}{dz}\chi(z) = \alpha_0\left[\chi_{\rm fid}(z)\left(\sum_{i=1}^{N}\frac{1}{(i-1)!}\alpha_i x^{i-1}\right)\frac{dx}{dz} + \left(1 + \sum_{i=1}^{N}\frac{1}{i!}\alpha_i x^i\right)\frac{d}{dz}\chi_{\rm fid}(z)\right],\\ &= \alpha_0\left[\chi_{\rm fid}(z)\left(\sum_{i=1}^{N}\frac{1}{(i-1)!}\alpha_i x^{i-1}\right)\frac{1}{H_{\rm fid}(z)\chi_{\rm fid}(z_{\rm p})} + \left(1 + \sum_{i=1}^{N}\frac{1}{i!}\alpha_i x^i\right)\frac{1}{H_{\rm fid}(z)}\right].\end{aligned} \tag{C3}$$

Then

$$\begin{aligned}\frac{H_{\rm fid}(z)}{H(z)} &= \alpha_0\left[\left(\sum_{i=1}^{N}\frac{1}{(i-1)!}\alpha_i x^{i-1}\right)\frac{\chi_{\rm fid}(z)}{\chi_{\rm fid}(z_{\rm p})} + \left(1 + \sum_{i=1}^{N}\frac{1}{i!}\alpha_i x^i\right)\right],\\ &= \alpha_0\left[\left(\sum_{i=1}^{N}\frac{1}{(i-1)!}\alpha_i x^{i-1}\right)(1+x) + \left(1 + \sum_{i=1}^{N}\frac{1}{i!}\alpha_i x^i\right)\right].\end{aligned} \tag{C4}$$

For the case of $N = 6$ for example,

$$\begin{aligned}&\frac{D_{\rm A}}{D_{\rm A,\ fid}}\\ &= \alpha_0\left(1 + \alpha_1 x + \frac{1}{2}\alpha_2 x^2 + \frac{1}{6}\alpha_3 x^3 + \frac{1}{24}\alpha_4 x^4 + \frac{1}{120}\alpha_5 x^5 + \frac{1}{720}\alpha_6 x^6\right),\end{aligned} \tag{C5}$$

$$\begin{aligned}\frac{H_{\rm fid}(z)}{H(z)} &= \alpha_0\left(\alpha_1 + \alpha_2 x + \frac{1}{2}\alpha_3 x^2 + \frac{1}{6}\alpha_4 x^3 + \frac{1}{24}\alpha_5 x^4 + \frac{1}{120}\alpha_6 x^5\right)(1+x)\\ &+\alpha_0\left(1 + \alpha_1 x + \frac{1}{2}\alpha_2 x^2 + \frac{1}{6}\alpha_3 x^3 + \frac{1}{24}\alpha_4 x^4 + \frac{1}{120}\alpha_5 x^5 + \frac{1}{720}\alpha_6 x^6\right).\end{aligned} \tag{C6}$$

References

Adame, A. G., Aguilar, J., Ahlen, S., et al. 2024, arXiv:2404.03002
Aghamousa, A., Aguilar, J., Ahlen, S., et al. 2016, arXiv:1611.00036
Aghanim, N., Akrami, Y., Ashdown, M., et al. 2020, A&A, 641, A6, [Erratum: Astron. Astrophys. N. 652, C4 (2021)]
Alam, S., Aubert, M., Avila, S., et al. 2021, PhRvD, 103, 083533
Alam, U., Sahni, V., Saini, T. D., & Starobinsky, A. A. 2003, MNRAS, 344, 1057
Caldwell, R. R., & Linder, E. V. 2005, PhRvL, 95, 141301
Chevallier, M., & Polarski, D. 2001, IJMPD, 10, 213
Chiba, T. 2009, PhRvD, 73, 063501, [Erratum: Phys. Rev. D 80, 129901 (2009)]
Clarkson, C., & Zunckel, C. 2010, PhRvL, 104, 211301
Clifton, T., Ferreira, P. G., Padilla, A., & Skordis, C. 2012, PhR, 513, 1
Cole, S., Percival, W. J., Peacock, J. A., et al. 2005, MNRAS, 362, 505
Copeland, E. J., Sami, M., & Tsujikawa, S. 2006, IJMPD, 15, 1753
Crittenden, R. G., Zhao, G.-B., Pogosian, L., Samushia, L., & Zhang, X. 2012, JCAP, 02, 048
DESI Collaboration, Adame, A. G., & Aguilar, J. 2023, AJ, 167, 62
Eisenstein, D. J., & Hu, W. 1998, ApJ, 496, 605
Eisenstein, D. J., Zehavi, I., Hogg, D. W., et al. 2005, ApJ, 633, 560
Feng, B., Wang, X.-L., & Zhang, X.-M. 2005, PhLB, 607, 35
Holsclaw, T., Alam, U., Sanso, B., et al. 2010, PhRvL, 105, 241302
Kaiser, N. 1987, MNRAS, 227, 1
Linder, E. V. 2003, PhRvL, 90, 091301
LSST Science Collaboration, Abell, P. A., Allison, J., et al. 2009, arXiv:0912.0201
Matos, I. S., Quartin, M., Amendola, L., Kunz, M., & Sturani, R. 2023, arXiv:2311.17176
Peacock, J. A., Cole, S., Norberg, P., et al. 2001, Nature, 410, 169
Perlmutter, S., Aldering, G., Goldhaber, G., et al. 1999, ApJ, 517, 565
Planck Collaboration, Aghanim, N., Akrami, Y., et al. 2020, A&A, 641, A6
Riess, A. G., Filippenko, A. V., Challis, P., et al. 1998, AJ, 116, 1009
Rose, B. M., Baltay, C., Hounsell, R., et al. 2021, arXiv:2111.03081
Sahni, V., Saini, T. D., Starobinsky, A. A., & Alam, U. 2003, JETP Lett., 77, 201
Sahni, V., & Starobinsky, A. 2006, IJMPD, 15, 2105
Scherrer, R. J. 2006, PhRvD, 73, 043502
Seikel, M., Clarkson, C., & Smith, M. 2012, JCAP, 06, 036
Spergel, D., Gehrels, N., Baltay, C., et al. 2015, arXiv:1503.03757
Spergel, D. N., Verde, L., Peiris, H. V., et al. 2003, ApJS, 148, 175
Stern, D., Jimenez, R., Verde, L., Kamionkowski, M., & Stanford, S. A. 2010, JCAP, 02, 008
Torrado, J., & Lewis, A. 2021, JCAP, 2021, 057
Wang, X., Gu, G., Mu, X., Yuan, S., & Zhao, G.-B. 2024, RAA, 24, 065002
Wang, Y., Pogosian, L., Zhao, G.-B., & Zucca, A. 2018, ApJL, 869, L8
Zhao, G.-B., Crittenden, R. G., Pogosian, L., & Zhang, X. 2012, PhRvL, 109, 171301
Zhao, G.-B., Raveri, M., Pogosian, L., et al. 2017, NatAs, 1, 627
Zhu, F., Padmanabhan, N., & White, M. 2015, MNRAS, 451, 236